

The fundamental plane of blazars based on the black hole spin-mass energy

Xu Zhang^{1*}, Dingrong Xiong^{2†}, Quanguai Gao^{1,3}, Guiqin Yang⁴

Fangwu Lu^{1,3}, Weiwei Na¹, Longhua Qin¹

¹ Department of Physics, Yuxi Normal University, Yuxi 653100, People's Republic of China

² Yunnan Observatories, Chinese Academy of Sciences, 396 Yangfangwang, Guandu District, Kunming, 650216, Peoples Republic of China

³ Key Laboratory of Astroparticle Physics of Yunnan Province, Kunming 650091, People's Republic of China

⁴ Faculty of Mechanical and Electrical Engineering, Kunming University of Science and Technology, Kunming 650031, People's Republic of China

15 March 2024

ABSTRACT

We examine the fundamental plane of 91 Blazars which include FS-RQs and BL Lacs with known X-ray luminosity (L_R), radio luminosity (L_X), and black hole mass measurements (M) to reflect the relationship between jet and accretion for blazars. The fundamental plane of Blazars are $\log L_R = 0.273_{+0.059}^{-0.059} \log L_X + 0.695_{+0.191}^{-0.191} \log M + 25.457_{+2.728}^{-2.728}$ and $\log L_R = 0.190_{+0.049}^{-0.049} \log L_X + 0.475_{+0.157}^{-0.157} \log M + 28.568_{+2.245}^{-2.245}$ after considering the effect of beam factor. Our results suggest that the jet of blazars has connection with accretion. We set the black hole spin energy as a new variable to correct the black hole mass and explore the effect of black hole spin on the fundamental relationship. We find that the fundamental plane of Blazars is effected by the black hole spin, which is similar to the previous work for AGNs. We additionally examine a new fundamental plane which is based on the black hole spin-mass energy (M_{spin}). The new fundamental plane ($\log L_R = 0.332_{+0.081}^{-0.081} \log L_X + 0.502_{+0.091}^{-0.091} \log M_{spin} + 22.606_{+3.346}^{-3.346}$ with R-Square=0.575) shows that M_{spin} has a better correlation coefficient comparing to the M for fundamental plane of Blazars. These results support that the black hole spin should be considered as a important factor for the study of fundamental plane for Blazars. And these may further our understanding of the Blandford-Znajek process in blazars.

Key words: accretion, accretion discs quasars: supermassive black holes black hole physics

1 INTRODUCTION

When studying the internal structure of binary star systems and galactic cores, the existence of a black hole (BH) can be inferred through various indirect indicators. These indicators show clear associations with black hole activity. One such indicator is the synchrotron radiation emitted by relativistic jets in the radio frequency range, while another common indicator is the intense and compact power-law X-ray emission, often associated with the inner regions of accretion disks (Begelman et al. 1984). It is widely observed that

the accretion of compact objects and the initiation of relativistic outflows/jets are interconnected phenomena (Falcke et al. 1994). This suggests an inherent correlation between the jet and disk accretion flux to some extent. To discuss this correlation, the concept of a fundamental plane relationship has been introduced. The fundamental plane for black hole activity is commonly defined as an approximate power-law relationship among the mass of BH, X-ray and radio luminosities. It usually applies to the hard state BHs. The applicability of fundamental plane for inclusion of soft or soft-intermediate state BHBs, as well as Seyferts is still not sure. This relationship applies to black holes that produce jets (Merloni et al. 2003; Falcke et al. 2004; Kording et al. 2006a,b; Gultekin et al. 2009; Unal et al. 2015). In black

* zx@yxnu.edu.cn

† xiongdingrong@ynao.ac.cn

holes with outflows and an accretion disk, X-ray luminosity is generally linked to accretion power, while radio luminosity reflects the jet power in radiatively inefficient active galactic nuclei (AGNs) which have sub-Eddington accretion rates (Heinz et al. 2003; Falcke et al. 2004; Merloni et al. 2003; Saikia et al. 2015; Kording et al. 2006a; Plotkin et al. 2012; Gultekin et al. 2009; Unal et al. 2015).

Blazars are the most extreme type of active galactic nuclei (AGNs), with their jets pointing towards the observer (Urry et al. 1995) and they constitute the brightest and most dominant population of AGNs in the gamma-ray band (Fichtel et al. 1994; Abdo et al. 2010). Their extreme observational properties are explained as a result of a beaming effect. Due to the relativistic beaming effect, the emission in the jet is strongly enhanced in the observer's frame (Urry et al. 1995). Blazars are typically divided into two sub-classes: BL Lacertae objects (BL Lacs) and flat spectrum radio quasars (FSRQs). FSRQs have strong emission lines, while BL Lacs objects have very weak or no emission lines. The classical division between FSRQs and BL Lacs is mainly based on the equivalent width (EW) of the emission lines. In a rest frame, objects with $EW > 5\text{\AA}$ are classified as FSRQs (e.g., Urry et al. 1995; Scarpa et al. 1997). Blandford et al. (1978) originally proposed that the absence of broad lines in BL Lacs is due to very bright, Doppler-enhanced continuous synchrotron radiation.

There is no consensus on the formation mechanism of relativistic jets until now. Three main mechanisms have been proposed to explain their formation. The first one is the Blandford-Znajek (BZ) mechanism, which posits that the rotational energy of the black hole and accretion disc are the primary source of the jets (Blandford et al. 1977). Furthermore, the jet power in the BZ mechanism is dependent on the spin of the black hole. The second mechanism is the Blandford-Payne (BP) mechanism, which suggests that the jet extracts the rotational energy of the accretion disc, and the mass of the black hole can be ignored. This mechanism has been supported by previous studies (Rawlings et al. 1991; Ghisellini et al. 2010; Gu et al. 2009; Cao et al. 1999; Tavecchio et al. 2010; Sbarrato et al. 2012; Ghisellini et al. 2014; Xiong et al. 2015; Begelman et al. 1984). Finally, A hybrid model for mixing BZ and BP mechanisms has been proposed by Meier et al. (2001) and Garofalo et al. (2010), which could provide an explanation for the observed differences in AGNs with relativistic jets (Garofalo et al. 2010). The jet power of Blazars often exceeds the luminosity of the accretion disk Ghisellini et al. (2014). It is shown that besides accretion, there are other important physical parameters that help to determine the jet power Meier et al. (2002), such as the spin and black hole mass of super-massive black holes. In particular, the spin of a black hole has often been speculated as the main parameter for determining the jet power of BH (Blandford et al. 1977). Unal et al. (2015) have examined the fundamental plane which confirmed that the jet energy scales quadratically with BH spin of AGN. Considering the involvement of BH spin in both accretion and jets, BH spin is crucial for the study of fundamental plane (Unal et al. 2015).

As a special type of AGN, Blazars should theoretically conform to the fundamental plane relation, which has been confirmed by previous studies (Merloni et al. 2003; Falcke et al. 2004; Bariuan et al. 2022; Unal et al. 2015; Saikia et al.

2015; Zhang et al. 2018). Merloni et al. (2003) and Falcke et al. (2004) examined the fundamental plane with a large sample including the blazars and confirmed that Blazars are also follow the fundamental plane of AGN. Saikia et al. (2016) used the intrinsic radio luminosity obtained through the Lorentz factor to calculate the fundamental plane of Blazars. Zhang et al. (2018) selected the radiatively efficient sources to get the fundamental plane of Blazars. In this paper, we conduct a fundamental analysis of blazars, and compare them with normal radio-loud and radio-quiet AGNs (Unal et al. 2015). Furthermore, we use a new calculation method (Daly et al. 2022) to incorporate black hole spin energy as a new variable to study the impact of black hole spin on the fundamental plane relation. The structure of this article is as follows. The sample is described in Section 2, and the analysis results are described in Section 3. Section 4 summarizes our conclusions.

2 THE SAMPLES

In order to do the fundamental plane of blazars, we tried to collect the sample of blazars as much as possible with reliable redshift, 2-10 keV X-ray luminosity, 5 GHz radio luminosity, BH mass, bolometric luminosity, beam power. For this purpose, we select the large samples of blazars from Ackermann et al. (2011) and Nolan et al. (2012) which can be detected by Very Large Array (VLA) for radio flux density and Swift or XMM-Newton for X-ray flux density. In order to collect as many sources as we need, we first obtain the samples following broad-line data of blazars (Cao et al. 1999; Wang et al. 2004; Liu et al. 2006; Sbarrato et al. 2012; Chai et al. 2012; Shen et al. 2011; Shaw et al. 2012). Secondly, we cross-correlated these sample with previous works (Woo et al. 2002; Xie et al. 2004; Liu et al. 2006; Zhou et al. 2009; Zhang et al. 2012; Sbarrato et al. 2012; Chai et al. 2012; Leon-Tavares et al. 2011; Shen et al. 2011; Shaw et al. 2012) to obtain the BH mass. At last, we selected the sample of blazars with radio flux density and X-ray flux density which are detected by VLA and Swift or XMM-Newton on NASA/IPAC Extragalactic Database (NED). The beaming factor of sample in this paper can be collected by cross-matching with the sources of Nemmen et al. (2012). In total, we collected a sample containing 91 blazars which includes 70 FSRQs and 21 BL Lacs. All sample of 91 Blazars with redshift (z), $\log M_{\text{dyn}}$, $\log L_X$, $\log L_R$, $\log L_{\text{bol}}$, $\log f_b$ and radio loudness (R) are listed in Table 1. We use the collected data to calculate the black hole spin energy (M_{spin}) and irreducible black hole mass (M_{irr}) of sample for further fundamental analysis. All sample of Blazars with $\log L_j$, $\log L_{\text{EDD}}$, $\log F$, $\log M_{\text{irr}}$, $\log M_{\text{spin}}$ are listed in Table 2. The sources are arranged in order of increasing redshift. The source distribution of Blazars' sample across several different physical properties is shown in Figure 1. The z and $\log R$ distributions of the various classes are shown in part a and b of Figure 1. The redshift distributions for all blazars are $0 \leq z \leq 2.6$ and mean value is 0.93. Mean values for FSRQs and BL Lacs are 1.07 and 0.44. The R distributions for all blazars are $10^{0.06} \leq R \leq 10^{4.96}$ and mean value is $10^{3.16}$. Mean values for FSRQs and BL Lacs are $10^{3.16}$ and $10^{2.70}$.

2.1 Black hole mass

The traditional virial BH mass also known as BH dynamical mass (M_{dyn}) of AGN usually could be measured by the empirical relationship between the BLR size and the ionization luminosity, as well as the measured wide line width, assuming that the BLR cloud is gravitationally bound by the central black hole (Xiong et al. 2014). In this paper we collected the BH mass of FSRQs which are estimated by traditional virial method (Woo et al. 2002; Wang et al. 2004; Liu et al. 2006; Shen et al. 2011; Chai et al. 2012; Sbarrato et al. 2012; Shaw et al. 2012). If the BH mass of sample can be attained from different lines, we take the average of BH masses from different lines. The BH masses we got from Vestergaard et al. (2006) attained by H β and C_{IV} lines, and Vestergaard et al. (2009) attained by Mg II lines. And for the BL Lac objects of sample, the masses of black holes can be estimated by the $M_{\text{BH}}-\sigma$ or $M_{\text{BH}}-L$ relationship of their host galaxies, where σ and L are the stellar velocity dispersion and the bulge luminosity of the host galaxy (Xiong et al. 2014; Woo et al. 2002; Zhou et al. 2009; Leon-Tavares et al. 2011; Chai et al. 2012; Sbarrato et al. 2012; Zhang et al. 2012). There is a little number of sources BH mass which are estimated by variation time-scale from Xie et al. (1991, 2004). If there are more than one BH masses we got that belong to the same sample, then we take the average of those data. The average difference for BH mass between the method of traditional virial and the properties of host galaxies from the same source is 0.023. Due to the small number of black hole masses estimated by varying time-scales, the difference between the black hole masses obtained from Xie et al. (1991, 2004) and other methods has little effect on the results. The BH mass distributions of the various classes are shown in part c of Figure 1. The BH mass distributions for all blazars are $10^{7.5} \sim 10^{10} M_{\odot}$ and mean value is $10^{8.70 \pm 0.30} M_{\odot}$. Mean values for FSRQs and BL Lacs are $10^{8.78 \pm 0.30} M_{\odot}$ and $10^{8.43 \pm 0.30} M_{\odot}$.

2.2 Intrinsic 5 GHz radio luminosity

In this paper, 5 GHz radio luminosity was calculated by 5 GHz radio flux density from NED. These radio fluxes were taken from 5 GHz high resolution VLA observations directly. In order to ensure the accuracy of the collected data and reduce errors caused by converting through other approximate frequency, we only collect sources that have accurate 5 GHz radio flux density. At the same time, we strive to make the observation time of the collected 5 GHz radio data align as closely as possible with the observation time of other bands, reducing errors caused by variations in observation time. If there is more than one observation from the same source, we take the average value of all observations. For different observations with the same wavelength from the same source, the difference is usually controlled between 0.03 and 0.12. After we averaged the difference, the error was basically controlled within 0.05. Blazars usually have very powerful relativistic jets which includes gamma-ray band and radio band. For this reason, We should consider the influence of the beaming effect (Xiong et al. 2014; Zhang et al. 2023a). The intrinsic luminosity of radio luminosity can be estimated by beaming factor f_b , $f_b = 1 - \cos\theta$ where θ is the jet opening angle (Nemmen et al. 2012; Zhang et al. 2017). The uncertainty of f_b

we took is 0.15 as reported in Nemmen et al. (2012).

$$f_b = 1 - \cos\theta_j, \quad (1)$$

θ_j is the jet opening angle of Blazars. The beaming factor f_b in this paper are obtained from Nemmen et al. (2012) and Xiong et al. (2014). we can measure the intrinsic 5 GHz radio luminosity with beaming factor.

$$L_{R^*} = L_R f_b, \quad (2)$$

L_{R^*} are the intrinsic luminosity of radio luminosity, respectively. The 5 GHz radio luminosity and beam factor distributions of the various classes are shown in part d and e of Figure 1. The 5 GHz radio luminosity distributions for all blazars are $10^{40} \sim 10^{46} \text{ erg s}^{-1}$ and mean value is $10^{43.95 \pm 0.05} \text{ erg s}^{-1}$. Mean values for FSRQs and BL Lacs are $10^{44.24 \pm 0.05} \text{ erg s}^{-1}$ and $10^{42.99 \pm 0.05} \text{ erg s}^{-1}$. The beam factor distributions for all blazars are $-4 \sim -1.25$ and mean value is -2.61 . Mean values for FSRQs and BL Lacs are -2.72 and -2.21 .

2.3 2-10 keV X-ray luminosity

To do the fundamental analysis of Blazars, the X-ray luminosity in 2-10 keV is required. In this paper, the X-ray luminosity in 2-10 keV was calculated by the X-ray flux density from NASA/IPAC Extragalactic Database (NED). In order to minimize errors caused by different observation devices, all data of X-ray flux density we choose are come from the same X-ray observation satellite as much as possible. Most of Blazars we collected can be observed by Swift with reliable data. Only a small number of samples did not have Swift observations, for these sources we collected the data of XMM-Newton. Most data of flux density in 2-10 keV can be obtained from the NED. But there are still some data that do not have the direct observational data in the 2-10 keV. Because of the limited number of X-ray flux densities with direct observational data in the 2-10 keV range, we only collected another 0.3-10 keV flux density directly observed by Swift, and used the power-law model to estimate the 2-10 keV flux density to expand the sample and reduce the error to a certain extent. The X-ray flux densities in 0.3-10 keV of Blazars from NED can be converted into 2-10 keV by the power-law model with photon index $\tau=1.87$ for FSRQs (Zhang et al. 2023b). The photon index we chose is the average photon index of Blazars which is similar to Sahakyan et al. (2021). Due to the small differences between two energy bands of X-rays, the uncertainty generated by the spectral index has little impact on the results.

$$\begin{aligned} F_{2-10\text{keV}} &= F_{0.3-10\text{keV}} \frac{\int_{2\text{keV}}^{10\text{keV}} \nu^{1-\tau} d\nu}{\int_{0.3\text{keV}}^{10\text{keV}} \nu^{1-\tau} d\nu} \\ &= F_{0.3-10\text{keV}} \times 0.5157, \end{aligned} \quad (3)$$

where $F_{2-10\text{keV}}$ and $F_{0.3-10\text{keV}}$ respectively are the X-ray flux density in 2-10 keV and 0.3-10 keV. ν is the energy dissipation of FSRQs. The 2-10keV X-ray luminosity distributions of the various classes are shown in part f of Figure 1. The 2-10keV X-ray luminosity distributions for all blazars are $10^{42.5} \sim 10^{47.5} \text{ erg s}^{-1}$ and mean value is $10^{45.58 \pm 0.35} \text{ erg s}^{-1}$. Mean values for FSRQs and BL Lacs are $10^{45.80 \pm 0.35} \text{ erg s}^{-1}$ and $10^{44.85 \pm 0.38} \text{ erg s}^{-1}$.

2.4 Black hole spin energy

The black hole spin energy was also considered as a variable for fundamental analysis. However, due to the limitations of observation and estimation methods, it is difficult to measure the spin of large black holes directly by conventional calculation methods. We measured the M_{spin} of BH with the method of [Daly et al. \(2022\)](#). The accuracy of this estimation method has been confirmed by previous work ([Daly et al. 2019](#)) which can consistent with previous works such as the X-ray reflection method ([Miller et al. 2009](#); [Reynolds et al. 2014](#)). To obtain the key data (Spin function F) of this method, the broad-line luminosity and the beam power of sample in this paper are required.

2.4.1 Bolometric luminosity

In this paper, the bolometric luminosity L_{bol} of our sample were collected from the previous work by cross matching. L_{BLR} which were collected from the previous work ([Xiong et al. 2014](#)) can be converted into L_{bol} ($L_{\text{bol}} = 10 L_{\text{BLR}}$) with an average uncertainty of 0.3dex ([Calderone et al. 2013](#)). According to [Celotti et al. \(1997\)](#), L_{BLR} usually were obtained by scaling several strong emission lines to the quasar template spectrum of [Francis et al. \(1991\)](#), with $L_{Y\alpha}$ as a reference. The luminosity of blazars emission lines in the Sloan Digital Sky Survey (SDSS) DR7 quasar sample ([Xiong et al. 2014](#)) can be converted to the total luminosity of the broad lines ([Sbarrato et al. 2012](#); [Celotti et al. 1997](#)). A proportions is set to estimate L_{BLR} by these method that the $L_{Y\alpha}$ flux contribution is set to 100 and the relative weights of $H\alpha$, $H\beta$, Mg_{II} and C_{IV} are 77, 22, 34 and 63, respectively. If there are more than one line was present, take the average of L_{BLR} estimated from each line. The uncertainty of $\log L_{\text{bol}}$ we took is 0.32 which is consistent with [Calderone et al. \(2013\)](#). The L_{bol} distributions of the various classes are shown in part g of Figure 1. The L_{bol} distributions for all blazars are $10^{42.5} \sim 10^{49.5} \text{ erg s}^{-1}$ and mean value is $10^{45.79 \pm 0.32} \text{ erg s}^{-1}$. Mean values for FSRQs and BL Lacs are $10^{46.07 \pm 0.32} \text{ erg s}^{-1}$ and $10^{44.85 \pm 0.32} \text{ erg s}^{-1}$.

2.4.2 Beam power

We used the theoretical model described by [Willott et al. \(1999\)](#) to calculate the beam power of our sample that replies on the relationships between beam power and radio luminosity at 151 MHz. For our sample, most of the 151 MHz radio luminosity directly comes from the Very Long Baseline Interferometry (VLBI) by cross-matching on NED. Only 6 FSRQ sources 151 MHz flux density has no direct observational data. Since the samples are all FSRQ, we collected the radio flux density at 140-160MHz for this sample and set the spectral index $\alpha = 1$ to measure the 151 MHz radio flux density. Because 151 MHz radio flux density are taken from extended radio flux density of samples. The correction factor can be negligible because the frequencies (140-160 MHz) are approximate.

$$L_j \approx 1.7 \times 10^{45} f^{3/2} \left(\frac{L_{151}}{10^{44} \text{ erg s}^{-1}} \right)^{6/7} \text{ erg s}^{-1}, \quad (4)$$

where L_{151} is the radio luminosity at 151 MHz in units of erg s^{-1} and L_j is the beam power. [Willott et al. \(1999\)](#) contended that the normalization is highly uncertain, prompting the introduction of the factor f to accommodate these uncertainties. The value range of f is $1 \leq f \leq 20$ ([Cao et al. 2003](#); [Godfrey et al. 2013](#); [Wu et al. 2008](#); [Fan et al. 2018, 2019](#)). According to analysis result of [Daly et al. \(2018\)](#) the uncertainty of beam power could be effected by the range of f . To reduce the uncertainty of our result as much as possible, we used the the lowest limit $f = 1$ to measured the beam power just like [Cao et al. \(2003\)](#). The L_{151} distributions of the various classes are shown in part h of Figure 1. The L_{151} distributions for all blazars are $10^{39.5} \sim 10^{45} \text{ erg s}^{-1}$ and mean value is $10^{42.85 \pm 0.03} \text{ erg s}^{-1}$. Mean values for FSRQs and BL Lacs are $10^{43.17 \pm 0.04} \text{ erg s}^{-1}$ and $10^{41.78 \pm 0.03} \text{ erg s}^{-1}$.

2.4.3 Spin function F

The spin function can be measured by the following formula ([Daly et al. 2022](#); [Zhang et al. 2023a](#)) with beam power, bolometric luminosity and Eddington luminosity we got.

$$\frac{f(j)}{f_{\text{max}}} = \left(\frac{L_j}{g_j L_{\text{Edd}}} \right) \left(\frac{L_{\text{bol}}}{g_{\text{bol}} L_{\text{Edd}}} \right)^{-A}, \quad (5)$$

where j is BH spin, L_{bol} is the bolometric luminosity ([Netzer et al. 1990](#)), L_{Edd} is the Eddington luminosity which can be measured by BH mass, $g_i = 0.1$ and $g_{\text{bol}} = 1$ are directly obtained from [Daly et al. \(2019\)](#), and A is a parameter defined by [Daly et al. \(2018\)](#), it can be measured by the coefficient of fundamental plane of BH ($A = a/(a+b)$), where a and b are the value of parameters from [Merloni et al. \(2003\)](#). In this paper, we set A as 0.43 ([Daly et al. 2018](#)). Based on the relationship among the black hole spin function F, the total mass M of BH (also known as M_{dyn}) and the spin-mass energy (M_{spin}) ([Blandford et al. 1990](#); [Thorne et al. 1986](#); [Rees et al. 1984](#); [Misner et al. 1973](#); [Zhang et al. 2023a](#)), we estimate M_{spin} by the black hole spin function F^2 . $M \equiv M_{\text{dyn}} = M_{\text{irr}} + E_{\text{spin}} c^{-2} = M_{\text{irr}} + M_{\text{spin}}$. [Daly et al. \(2022\)](#) showed that

$$\frac{M_{\text{irr}}}{M_{\text{dyn}}} = (F^2 + 1)^{-1/2},$$

$$\frac{M_{\text{spin}}}{M_{\text{dyn}}} = 1 - \frac{M_{\text{irr}}}{M_{\text{dyn}}} = [1 - (F^2 + 1)^{-1/2}], \quad (6)$$

where F is the spin function, $F^2 \equiv f(j)/f_{\text{max}}$ ([Daly et al. 2022](#)), M_{dyn} is the dynamic black hole mass and M_{irr} is the irreducible black hole mass.

3 THE RESULTS

3.1 fundamental plane of blazars

To examine the fundamental plane of Blazars, we should first explore the correlation between radio luminosity (L_R), X-ray luminosity (L_X), and black hole mass (M) which also can be converted to Eddington luminosity L_{Edd} . We use the method of [Merloni et al. \(2003\)](#) to determine the exist of fundamental plane. The results of the best fit is showed in Table 3. We found that the fundamental plane exists for

[htbp]

Table 1. The fundamental plane of Blazars

[1] name	[2] type	[3] z	[4] $\log M_{\text{dyn}}$	[5] $\log L_X$	[6] $\log L_R$	[7] $\log f_b$	[8] $\log R$
0106+013/4C+01.02	FSRQ	2.099	8.830 ± 0.300	46.460 ± 0.415	45.234 ± 0.003	-3.208	3.991
0110+495	FSRQ	0.389	8.340 ± 0.300	44.567 ± 0.370	42.966 ± 0.102	-2.221	3.536
0133+476/OC 457	FSRQ	0.859	8.515 ± 0.300	45.623 ± 0.414	44.462 ± 0.017	-2.618	3.752
0135-247/PKS0135-247	FSRQ	0.835	9.120 ± 0.300	45.695 ± 0.404	44.131 ± 0.022	-2.623	4.200
0234+285/4C +28.07	FSRQ	1.213	9.220 ± 0.300	46.064 ± 0.409	44.642 ± 0.007	-2.516	3.502
0235+164/PKS 0235+164	Bllac	0.940	9.073 ± 0.300	45.882 ± 0.426	44.005 ± 0.034	-2.467	2.966
0336-019/PKS 0336-01	FSRQ	0.852	8.935 ± 0.300	45.503 ± 0.413	44.434 ± 0.005	-3.032	3.584
0403-132/PKS 0403-13	FSRQ	0.571	9.075 ± 0.300	45.605 ± 0.320	44.108 ± 0.016	-2.703	3.616
0420-014/PKS 0420-01	FSRQ	0.916	8.813 ± 0.300	45.827 ± 0.434	44.663 ± 0.003	-2.400	3.196
0458-020/PKS 0458-020	FSRQ	2.291	8.965 ± 0.300	46.593 ± 0.408	45.284 ± 0.011	-2.741	3.996
0528+134	FSRQ	2.060	9.800 ± 0.300	46.604 ± 0.423	45.031 ± 0.027	-2.962	4.172
OG 050	Bllac	1.254	8.430 ± 0.350	45.989 ± 0.408	44.587 ± 0.026	-2.886	3.739
0537-441/PKS 0537-441	Bllac	0.892	8.565 ± 0.300	46.173 ± 0.032	44.576 ± 0.022	-2.829	3.086
0605-085/PKS 0605-085	FSRQ	0.872	8.628 ± 0.300	45.648 ± 0.406	44.357 ± 0.022	-3.009	3.087
0637-752/PKS 0637-75	FSRQ	0.653	9.110 ± 0.300	45.782 ± 0.421	44.404 ± 0.022	-2.782	3.482
B3 0650+453	FSRQ	0.928	8.170 ± 0.340	45.248 ± 0.377	43.369 ± 0.239	-2.475	3.340
0716+714	Bllac	0.300	8.100 ± 0.300	45.269 ± 0.431	43.151 ± 0.087	-2.319	2.316
0735+178	Bllac	0.424	8.300 ± 0.300	44.499 ± 0.399	43.145 ± 0.061	-2.504	3.058
0736+017/PKS 0736+01	FSRQ	0.189	8.110 ± 0.300	44.468 ± 0.424	42.864 ± 0.052	-2.736	3.111
0748+126/PKS 0748+126	FSRQ	0.889	8.150 ± 0.300	45.837 ± 0.409	44.524 ± 0.015	-2.675	3.541
0754+100	Bllac	0.266	8.200 ± 0.300	44.731 ± 0.418	42.865 ± 0.042	-2.974	2.514
PKS0808+019	Bllac	1.148	8.500 ± 0.300	45.265 ± 0.366	44.388 ± 0.035	-2.615	3.583
4C +39.23	FSRQ	1.216	8.550 ± 0.300	45.544 ± 0.326	44.245 ± 0.068	-2.779	3.046
OJ 535	FSRQ	1.418	9.260 ± 0.300	45.902 ± 0.378	44.375 ± 0.054	-2.822	3.187
0823+033/PKS 0823+033	Bllac	0.506	8.830 ± 0.300	44.967 ± 0.407	43.699 ± 0.058	-2.486	2.641
B2 0827+24	FSRQ	0.940	8.953 ± 0.300	46.004 ± 0.424	44.087 ± 0.039	-3.104	3.024
PKS 0829+046	Bllac	0.174	8.630 ± 0.300	43.919 ± 0.415	42.403 ± 0.073	-2.111	2.126
OJ 451	FSRQ	0.249	9.680 ± 0.090	43.805 ± 0.315	42.252 ± 0.087	-1.972	2.367
0836+710/4C+71.07	FSRQ	2.172	9.360 ± 0.300	47.483 ± 0.012	44.950 ± 0.031	-3.198	2.859
0851+202/OJ 287	Bllac	0.306	8.563 ± 0.300	45.009 ± 0.431	43.418 ± 0.022	-2.229	2.792
S4 0859+470	FSRQ	1.466	9.250 ± 0.030	45.632 ± 0.320	44.529 ± 0.011	-2.863	3.645
0906+015/PKS 0906+01	FSRQ	1.024	9.003 ± 0.300	45.871 ± 0.415	44.115 ± 0.056	-2.617	2.889
S4 0913+39	FSRQ	1.267	8.620 ± 0.150	45.193 ± 0.320	43.968 ± 0.074	-2.727	3.237
B3 0917+449	FSRQ	2.190	9.283 ± 0.300	46.758 ± 0.406	44.740 ± 0.051	-2.893	2.792
OK 630	FSRQ	1.453	8.930 ± 0.160	45.819 ± 0.375	44.557 ± 0.037	-2.760	3.678
4C +40.24	FSRQ	1.249	8.950 ± 0.060	45.717 ± 0.375	44.487 ± 0.074	-3.275	3.471
0953+254/B2 0954+25A	FSRQ	0.707	8.876 ± 0.300	45.256 ± 0.405	43.602 ± 0.099	-2.555	3.252
4C+55.17	FSRQ	0.896	8.338 ± 0.300	45.159 ± 0.023	43.764 ± 0.020	-2.800	2.848
4C+23.24	FSRQ	0.566	8.510 ± 0.098	45.098 ± 0.362	43.636 ± 0.079	-2.483	3.117
1ES 1011+496	Bllac	0.212	8.300 ± 0.300	45.398 ± 0.429	42.015 ± 0.259	-1.987	1.627
1055+018/PKS 1055+01	Bllac	0.888	8.410 ± 0.300	45.881 ± 0.422	44.605 ± 0.015	-2.190	3.660
Mkn 421	Bllac	0.03	8.153 ± 0.300	44.990 ± 0.320	40.399 ± 0.066	-1.459	0.060
1127-145	FSRQ	1.184	9.180 ± 0.300	46.657 ± 0.017	44.975 ± 0.039	-2.984	3.365
4C+29.45	FSRQ	0.724	8.499 ± 0.300	45.458 ± 0.419	43.911 ± 0.045	-3.100	3.323
1202-262/PKS 1203-26	FSRQ	0.789	8.795 ± 0.300	45.602 ± 0.320	43.937 ± 0.015	-2.660	3.982
1219+285	Bllac	0.102	7.700 ± 0.300	43.606 ± 0.425	41.563 ± 0.163	-1.850	1.514
4C+04.42	FSRQ	0.965	8.305 ± 0.300	45.956 ± 0.409	43.754 ± 0.078	-2.607	1.702
4C+21.35	FSRQ	0.432	8.737 ± 0.300	45.263 ± 0.320	43.225 ± 0.116	-3.609	2.580
1226+023/3C 273	FSRQ	0.158	8.510 ± 0.300	45.723 ± 0.430	44.087 ± 0.005	-2.581	2.580
1253-055/3C 279	FSRQ	0.536	8.503 ± 0.300	45.922 ± 0.431	44.660 ± 0.005	-2.937	3.451
1308+326/B2 1308+32	FSRQ	0.996	8.478 ± 0.300	45.823 ± 0.414	44.185 ± 0.018	-2.986	3.982
B2 1315+34A	FSRQ	1.056	9.215 ± 0.300	45.208 ± 0.308	43.556 ± 0.200	-2.568	3.464
B2 1324+22	FSRQ	1.4	9.245 ± 0.300	46.011 ± 0.150	44.426 ± 0.047	-2.376	3.033
1334-127/PKS 1335-127	FSRQ	0.539	7.980 ± 0.300	45.580 ± 0.416	44.195 ± 0.018	-2.611	3.516
B3 1343+451	FSRQ	2.534	8.980 ± 0.990	46.398 ± 0.043	44.363 ± 0.157	-2.733	3.543
S5 1357+76	FSRQ	1.585	8.255 ± 0.210	45.409 ± 0.339	44.106 ± 0.123	-2.726	3.501
B3 1417+385	FSRQ	1.831	8.620 ± 0.250	45.799 ± 0.387	44.713 ± 0.039	-2.759	3.639
PKS 1434+235	FSRQ	1.548	8.375 ± 0.300	45.776 ± 0.324	44.237 ± 0.087	-2.756	3.739
PKS 1502+106	FSRQ	1.839	9.107 ± 0.300	46.221 ± 0.410	44.609 ± 0.051	-2.665	3.355

Note: The first column is name; the second column is type of blazars; the third column is redshift; the fourth column is the Logarithm of Black hole dynamical mass; the fifth column is Logarithm of x-ray luminosity in 2-10 keV (in units of erg s^{-1}); the sixth column is Logarithm of 5 GHz radio luminosity (in units of erg s^{-1}); the seventh column is Logarithm of the beaming factor; the eighth column is Logarithm of the radio loudness.

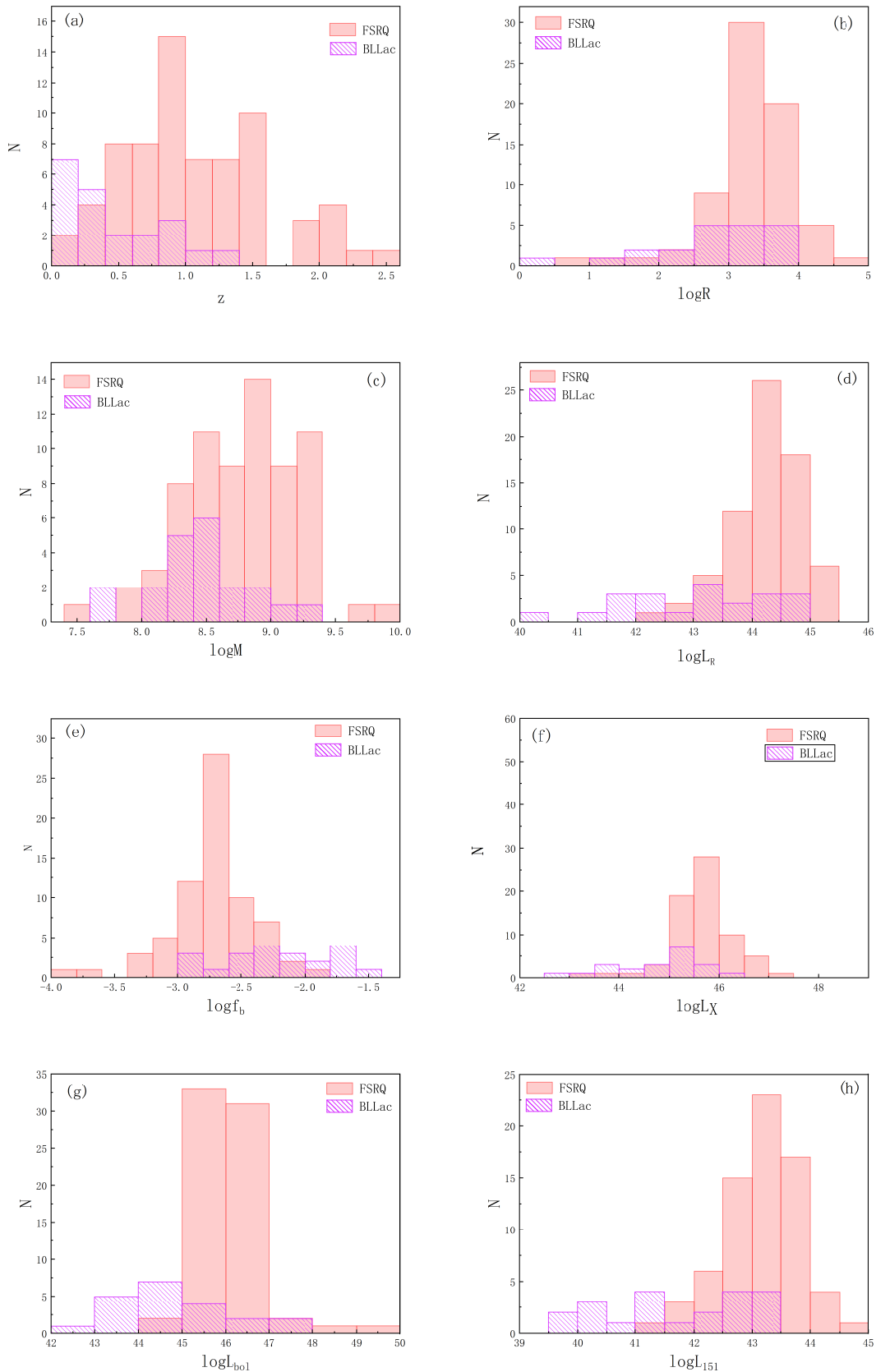


Figure 1. Distribution of the FSRQ and BL Lacs samples used in our study of fundamental plane for blazars. Histograms illustrate the distribution of several different physical properties, including: (a) redshift z , (b) radio loudness $\log R$, (c) black hole mass $\log M$, (d) 5 GHz radio luminosity $\log L_R$, (e) beam factor $\log f_b$, (f) 2-10 keV X-ray luminosity $\log L_X$, (g) bolometric luminosity $\log L_{bol}$, (h) 151 MHz radio luminosity $\log L_{151}$.

Table 1. continued

[1] name	[2] type	[3] z	[4] $\log M_{\text{dyn}}$	[5] $\log L_X$	[6] $\log L_R$	[7] $\log f_b$	[8] $\log R$
1508-055	FSRQ	1.185	8.970 ± 0.300	45.578 ± 0.035	44.606 ± 0.022	-2.912	3.335
1510-089/PKS 1510-08	FSRQ	0.361	8.363 ± 0.300	45.426 ± 0.028	43.709 ± 0.031	-2.929	3.259
1514-241	Bllac	0.049	7.650 ± 0.300	43.224 ± 0.419	41.912 ± 0.022	-1.776	3.336
B2 1520+31	FSRQ	1.484	8.920 ± 0.310	45.506 ± 0.342	44.089 ± 0.113	-2.606	1.344
1546+027/PKS 1546+027	FSRQ	0.414	8.618 ± 0.300	44.918 ± 0.422	43.490 ± 0.035	-2.336	3.628
4C+05.64	FSRQ	1.422	9.180 ± 0.300	45.972 ± 0.386	44.908 ± 0.090	-2.897	3.081
4C+10.45	FSRQ	1.226	8.970 ± 0.300	45.900 ± 0.434	44.316 ± 0.039	-2.854	4.001
1611+343/B2 1611+34	FSRQ	1.397	9.343 ± 0.300	45.899 ± 0.405	44.847 ± 0.018	-2.108	3.421
1622-297	FSRQ	0.815	9.100 ± 0.300	45.408 ± 0.320	44.228 ± 0.026	-2.721	3.371
1633+382/4C+38.41	FSRQ	1.814	9.369 ± 0.300	46.718 ± 0.427	45.090 ± 0.024	-3.287	2.910
4C +47.44	FSRQ	0.735	8.565 ± 0.475	45.330 ± 0.371	43.655 ± 0.077	-2.564	3.455
Mkn 501	Bllac	0.034	8.837 ± 0.300	44.210 ± 0.431	41.236 ± 0.053	-1.613	3.596
B3 1708+433	FSRQ	1.027	7.920 ± 0.350	45.110 ± 0.314	43.264 ± 0.372	-2.350	0.819
1726+455	FSRQ	0.717	8.220 ± 0.300	45.054 ± 0.395	43.826 ± 0.050	-2.532	2.870
1730-130	FSRQ	0.902	9.300 ± 0.300	45.615 ± 0.418	44.851 ± 0.007	-3.934	3.013
1739+522	FSRQ	1.375	9.320 ± 0.300	46.028 ± 0.402	44.404 ± 0.086	-2.718	4.961
4C+09.57/PKS1749+096	Bllac	0.322	8.413 ± 0.300	45.019 ± 0.422	43.449 ± 0.026	-2.097	2.845
CGRaBS J1800+7828/S5 1803+78	Bllac	0.68	8.260 ± 0.300	45.498 ± 0.419	44.133 ± 0.022	-2.248	3.179
3C 371	Bllac	0.051	8.605 ± 0.300	42.956 ± 0.423	41.524 ± 0.033	-1.775	3.092
1823+568/4C+56.27	Bllac	0.664	9.260 ± 0.300	45.458 ± 0.407	43.763 ± 0.016	-2.319	1.144
1849+670/CGRaBS J1849+6705	FSRQ	0.657	9.140 ± 0.300	45.270 ± 0.411	43.845 ± 0.040	-2.412	3.047
1921-293/PKS B1921-293	FSRQ	0.353	8.695 ± 0.300	45.320 ± 0.414	44.341 ± 0.005	-2.729	3.085
2145+067/4C+06.69	FSRQ	0.99	8.870 ± 0.300	46.225 ± 0.422	44.892 ± 0.008	-2.097	4.042
2155-152/PKS 2155-152	FSRQ	0.672	7.590 ± 0.300	45.307 ± 0.414	44.237 ± 0.022	-2.703	3.250
BL Lac	Bllac	0.069	8.210 ± 0.300	43.828 ± 0.320	42.048 ± 0.030	-1.767	3.861
PKS 2209+236	FSRQ	1.125	8.460 ± 0.450	45.217 ± 0.398	44.150 ± 0.058	-2.597	2.265
2223-052/3C 446	FSRQ	1.404	8.417 ± 0.300	43.176 ± 0.320	45.186 ± 0.011	-2.636	4.115
PKS 2227-08	FSRQ	1.56	8.785 ± 0.300	46.420 ± 0.402	44.845 ± 0.014	-2.301	3.712
2230+114/CTA 102	FSRQ	1.037	8.780 ± 0.300	46.268 ± 0.320	44.937 ± 0.036	-2.676	3.331
2251+158/3C 454.3	FSRQ	0.859	8.825 ± 0.300	46.884 ± 0.320	45.013 ± 0.013	-2.881	3.677
TXS 2331+073	FSRQ	0.401	8.370 ± 0.500	44.780 ± 0.408	43.255 ± 0.023	-2.281	3.495
2345-16/PKS 2345-16	FSRQ	0.576	8.595 ± 0.300	45.369 ± 0.413	44.007 ± 0.022	-2.631	2.974

Note: The first column is name; the second column is type of blazars; the third column is redshift; the fourth column is the Logarithm of Black hole dynamical mass; the fifth column is Logarithm of x-ray luminosity in 2-10 keV (in units of erg s^{-1}); the sixth column is Logarithm of 5 GHz radio luminosity (in units of erg s^{-1}); the seventh column is Logarithm of the beaming factor; the eighth column is Logarithm of the radio loudness.

Blazars, just as previous research has shown for AGN (Merloni et al. 2003; Unal et al. 2015; Bariuan et al. 2022). This means that there is a correlation between L_X/L_{Edd} and L_R (Merloni et al. 2003; Zhang et al. 2018). And we found the best fit of blazars is very similar to radio-loud quasars (RL). The data points are distributed along the direction of the extended line of fit. This confirms the current theoretical classification of Blazars as a subtype of radio-loud active galactic nuclei. After correcting for the beam effect, the radio data points of FSRQs change from near the radio loud quasar region ($\log L_R = 42.5-45$) with average value 45.26 to near the radio quiet quasar region after correcting for the beam effect ($\log L_R = 39.5-43$) with average value 42.65. It suggests that the differences for Blazars between left plane and right plane of Figure 2 may be caused by the beaming effect induced by relativistic jets. This further underscores the importance of accounting for beaming effects when conducting fundamental plane analysis of Blazars.

In this paper, the fundamental plane of Blazars we defined is consistent with Merloni et al. (2003). We use a multiple linear regression equation to obtain the fundamental

relationship and verify its reliability.

$$\log L_R = a \log L_X + b \log M + c, \quad (7)$$

where L_R is 5 GHz luminosity, L_X is the X-ray luminosity in 2-10 keV, M is the BH mass of Blazars. a and b and c are fitting parameters (Zhang et al. 2018). Multiple linear regression analysis was performed to obtain the best fitting linear regression coefficient (Merloni et al. 2003; Kording et al. 2006a; Zhang et al. 2018, 2023a). Linear regression analysis enables the derivation of three variables, namely a , b , and c , each with associated errors (Wang et al. 2017). The fundamental plane for Blazars, $\log L_R = 0.273_{+0.059}^{-0.059} \log L_X + 0.695_{+0.191}^{-0.191} \log M + 25.457_{+2.728}^{-2.728}$ with R-Square=0.355, is showed in left plane of Figure 3. We examined the fundamental plane relation for Blazars. It shows that the jet energy of Blazars has a correlation with accretion and spin of BH. It is consistent with the theory of BZ model (Blandford et al. 1977). Due to the strong relativistic jets of Blazars, 5 GHz radio luminosity originating from jet can be affected by the beaming effect. It may influence the analysis results of the fundamental plane. Therefore, we measured the intrinsic 5 GHz radio luminosity for

Table 2. The BH spin energy of Blazars

[1] name	[2] $\log L_{151}$	[3] $\log L_j$	[4] $\log L_{\text{Edd}}$	[5] $\log L_{\text{bol}}$	[6] $\log F$	[7] $\log M_{\text{spin}}$	[8] $\log M_{\text{irr}}$
0106+013/4C+01.02	44.378 ± 0.036	45.171 ± 0.031	46.944 ± 0.300	47.135	-0.428 ± 0.129	8.767 ± 0.243	7.962 ± -0.613
0110+495	42.027 ± 0.036	43.540 ± 0.031	46.454 ± 0.300	45.780	-0.812 ± 0.129	8.335 ± 0.285	6.407 ± -1.155
0133+476/OC 457	42.877 ± 0.022	44.268 ± 0.019	46.629 ± 0.300	45.444	-0.426 ± 0.141	8.486 ± 0.263	7.320 ± -0.790
0135-247/PKS0135-247	43.415 ± 0.036	44.729 ± 0.031	47.234 ± 0.300	46.343	-0.561 ± 0.129	9.104 ± 0.273	7.673 ± -0.912
0234+285/4C +28.07	43.451 ± 0.036	44.760 ± 0.031	47.334 ± 0.300	46.244	-0.553 ± 0.129	9.204 ± 0.272	7.789 ± -0.905
0235+164/PKS 0235+164	42.839 ± 0.036	44.235 ± 0.031	47.187 ± 0.300	44.920	-0.489 ± 0.129	9.052 ± 0.268	7.762 ± -0.844
0336-019/PKS 0336-01	42.903 ± 0.036	44.290 ± 0.031	47.049 ± 0.300	46.000	-0.654 ± 0.129	8.925 ± 0.278	7.310 ± -1.001
0403-132/PKS 0403-13	43.272 ± 0.036	44.607 ± 0.031	47.189 ± 0.300	46.250	-0.589 ± 0.129	9.061 ± 0.274	7.575 ± -0.939
0420-014/PKS 0420-01	43.049 ± 0.036	44.415 ± 0.031	46.927 ± 0.300	45.901	-0.535 ± 0.129	8.796 ± 0.271	7.415 ± -0.888
0458-020/PKS 0458-020	44.385 ± 0.036	45.560 ± 0.031	47.079 ± 0.300	46.304	-0.093 ± 0.129	8.856 ± 0.224	8.312 ± -0.492
0528+134	43.443 ± 0.036	44.753 ± 0.031	47.914 ± 0.300	49.650	-1.454 ± 0.129	9.800 ± 0.296	6.591 ± -1.790
OG 050	43.407 ± 0.036	44.722 ± 0.031	46.544 ± 0.350	45.864	-0.265 ± 0.129	8.374 ± 0.298	7.515 ± -0.385
0537-441/PKS 0537-441	43.297 ± 0.036	44.628 ± 0.031	46.679 ± 0.300	46.020	-0.384 ± 0.129	8.531 ± 0.259	7.445 ± -0.746
0605-085/PKS 0605-085	43.257 ± 0.036	44.593 ± 0.031	46.741 ± 0.300	45.600	-0.329 ± 0.129	8.584 ± 0.254	7.604 ± -0.695
0637-752/PKS 0637-75	43.737 ± 0.036	45.005 ± 0.031	47.224 ± 0.300	46.228	-0.395 ± 0.129	9.077 ± 0.260	7.969 ± -0.757
B3 0650+453	42.552 ± 0.057	43.989 ± 0.049	46.284 ± 0.340	45.260	-0.427 ± 0.111	8.142 ± 0.303	6.972 ± -0.655
0716+714	41.993 ± 0.007	43.510 ± 0.006	46.214 ± 0.300	45.766	-0.756 ± 0.154	8.093 ± 0.283	6.278 ± -1.112
0735+178	42.386 ± 0.036	43.847 ± 0.031	46.414 ± 0.300	47.600	-1.038 ± 0.129	8.298 ± 0.291	5.920 ± -1.378
0736+017/PKS 0736+01	41.635 ± 0.036	43.203 ± 0.031	46.224 ± 0.300	45.195	-0.789 ± 0.129	8.104 ± 0.284	6.223 ± -1.133
0748+126/PKS 0748+126	43.010 ± 0.036	44.382 ± 0.031	46.264 ± 0.300	45.950	-0.374 ± 0.129	8.114 ± 0.258	7.048 ± -0.736
0754+100	41.417 ± 0.036	43.017 ± 0.031	46.314 ± 0.300	47.500	-1.404 ± 0.129	8.200 ± 0.296	5.091 ± -1.740
PKS0808+019	42.817 ± 0.036	44.216 ± 0.031	46.614 ± 0.300	44.623	-0.271 ± 0.129	8.445 ± 0.247	7.574 ± -0.644
4C +39.23	43.760 ± 0.016	45.025 ± 0.013	46.664 ± 0.300	45.834	-0.141 ± 0.147	8.459 ± 0.232	7.828 ± -0.540
OJ 535	43.615 ± 0.017	44.900 ± 0.015	47.374 ± 0.300	46.302	-0.506 ± 0.146	9.240 ± 0.269	7.916 ± -0.868
0823+033/PKS 0823+033	42.039 ± 0.036	43.550 ± 0.031	46.944 ± 0.300	44.374	-0.644 ± 0.129	8.819 ± 0.277	7.224 ± -0.992
B2 0827+24	42.679 ± 0.036	44.098 ± 0.031	47.066 ± 0.300	45.989	-0.752 ± 0.129	8.946 ± 0.282	7.136 ± -1.097
PKS 0829+046	41.317 ± 0.036	42.931 ± 0.031	46.744 ± 0.300	43.568	-0.724 ± 0.129	8.622 ± 0.281	6.870 ± -1.069
OJ 451	41.105 ± 0.069	42.749 ± 0.059	47.794 ± 0.090	44.070	-1.222 ± 0.101	9.679 ± 0.083	6.934 ± -2.677
0836+710/4C+71.07	44.378 ± 0.008	45.555 ± 0.007	47.474 ± 0.300	47.430	-0.450 ± 0.153	9.334 ± 0.266	8.120 ± -0.819
0851+202/OJ 287	41.489 ± 0.036	43.078 ± 0.031	46.677 ± 0.300	44.580	-0.849 ± 0.129	8.559 ± 0.286	6.559 ± -1.191
S4 0859+470	43.945 ± 0.010	45.183 ± 0.009	47.364 ± 0.030	46.264	-0.354 ± 0.151	9.211 ± -0.021	8.183 ± -0.389
0906+015/PKS 0906+01	42.962 ± 0.036	44.341 ± 0.031	47.117 ± 0.300	46.100	-0.669 ± 0.129	8.994 ± 0.279	7.349 ± -1.017
S4 0913+39	43.498 ± 0.021	44.800 ± 0.018	46.734 ± 0.150	45.804	-0.267 ± 0.143	8.564 ± 0.092	7.701 ± -0.339
B3 0917+449	43.867 ± 0.034	45.117 ± 0.029	47.397 ± 0.300	46.850	-0.523 ± 0.132	9.265 ± 0.270	7.909 ± -0.877
OK 630	43.334 ± 0.015	44.660 ± 0.013	47.044 ± 0.160	46.055	-0.479 ± 0.147	8.907 ± 0.125	7.636 ± -0.691
4C +40.24	43.615 ± 0.036	44.900 ± 0.031	47.064 ± 0.060	46.502	-0.461 ± 0.129	8.925 ± 0.020	7.690 ± -0.459
0953+254/B2 0954+25A	42.311 ± 0.061	43.783 ± 0.053	46.990 ± 0.300	45.950	-0.880 ± 0.108	8.873 ± 0.286	6.810 ± -1.211
4C+55.17	43.535 ± 0.007	44.832 ± 0.006	46.451 ± 0.300	45.574	-0.121 ± 0.155	8.239 ± 0.230	7.644 ± -0.527
4C+23.24	42.771 ± 0.020	44.177 ± 0.017	46.623 ± 0.098	45.893	-0.566 ± 0.143	8.494 ± 0.067	7.053 ± -0.744
1ES 1011+496	41.067 ± 0.028	42.717 ± 0.024	46.414 ± 0.300	46.505	-1.368 ± 0.136	8.300 ± 0.296	5.262 ± -1.708
1055+018/PKS 1055+01	43.494 ± 0.036	44.796 ± 0.031	46.524 ± 0.300	45.509	-0.146 ± 0.129	8.320 ± 0.231	7.681 ± -0.535
Mkn 421	39.712 ± 0.028	41.555 ± 0.024	46.266 ± 0.300	42.699	-1.089 ± 0.137	8.151 ± 0.292	5.672 ± -1.431
1127-145	43.664 ± 0.036	44.942 ± 0.031	47.294 ± 0.300	46.770	-0.563 ± 0.129	9.164 ± 0.273	7.729 ± -0.914
4C+29.45	43.151 ± 0.020	44.502 ± 0.017	46.613 ± 0.300	45.710	-0.361 ± 0.143	8.461 ± 0.258	7.419 ± -0.732
1202-262/PKS 1203-26	43.428 ± 0.036	44.740 ± 0.031	46.909 ± 0.300	45.070	-0.189 ± 0.129	8.719 ± 0.237	8.001 ± -0.572
1219+285	40.336 ± 0.053	42.090 ± 0.045	45.814 ± 0.300	43.250	-0.811 ± 0.115	7.695 ± 0.284	5.770 ± -1.147
4C+04.42	43.230 ± 0.036	44.571 ± 0.031	46.419 ± 0.300	45.857	-0.303 ± 0.129	8.257 ± 0.251	7.325 ± -0.673
4C+21.35	42.783 ± 0.018	44.187 ± 0.015	46.851 ± 0.300	46.209	-0.694 ± 0.145	8.728 ± 0.280	7.035 ± -1.048
1226+023/3C 273	42.983 ± 0.036	44.359 ± 0.031	46.624 ± 0.300	46.540	-0.615 ± 0.129	8.498 ± 0.276	6.961 ± -0.964
1253-055/3C 279	43.557 ± 0.036	44.851 ± 0.031	46.616 ± 0.300	45.610	-0.166 ± 0.129	8.420 ± 0.234	7.742 ± -0.553
1308+326/B2 1308+32	43.062 ± 0.019	44.426 ± 0.017	46.591 ± 0.300	46.090	-0.475 ± 0.144	8.454 ± 0.267	7.192 ± -0.838
B2 1315+34A	43.105 ± 0.036	44.463 ± 0.030	47.329 ± 0.300	46.070	-0.662 ± 0.130	9.205 ± 0.278	7.574 ± -1.010
B2 1324+22	42.928 ± 0.036	44.311 ± 0.031	47.359 ± 0.300	45.896	-0.709 ± 0.129	9.237 ± 0.280	7.513 ± -1.055
1334-127/PKS 1335-127	42.782 ± 0.036	44.187 ± 0.031	46.094 ± 0.300	45.180	-0.257 ± 0.129	7.922 ± 0.246	7.077 ± -0.631
B3 1343+451	43.223 ± 0.089	44.565 ± 0.076	47.094 ± 0.990	46.120	-0.555 ± 0.084	8.964 ± 0.971	7.544 ± -2.038
S5 1357+76	42.802 ± 0.064	44.204 ± 0.055	46.369 ± 0.210	45.200	-0.331 ± 0.105	8.212 ± 0.160	7.227 ± -0.351
B3 1417+385	43.197 ± 0.036	44.542 ± 0.031	46.734 ± 0.250	46.104	-0.461 ± 0.129	8.595 ± 0.214	7.361 ± -0.694
PKS 1434+235	43.078 ± 0.062	44.440 ± 0.053	46.489 ± 0.300	45.775	-0.371 ± 0.107	8.339 ± 0.257	7.277 ± -0.724
PKS 1502+106	43.488 ± 0.036	44.792 ± 0.031	47.221 ± 0.300	46.297	-0.516 ± 0.129	9.087 ± 0.270	7.745 ± -0.869

Note: The first column is name; the second column is Logarithm of 151 MHz radio luminosity; the third column is Logarithm of beam power; the fourth column is the Logarithm of Eddington luminosity; the fifth column is Logarithm of the beaming factor; the sixth column is the Logarithm of the spin function; the seventh column is the Logarithm of black hole spin-mass energy; the eighth column is Logarithm of the black hole irreducible mass.

Table 2. continued

[1] name	[2] $\log L_{151}$	[3] $\log L_j$	[4] $\log L_{\text{Edd}}$	[5] $\log L_{\text{bol}}$	[6] $\log F$	[7] $\log M_{\text{spin}}$	[8] $\log M_{\text{irr}}$
1508-055	44.229 ± 0.036	45.426 ± 0.031	47.084 ± 0.300	46.520	-0.208 ± 0.129	8.899 ± 0.240	8.147 ± -0.588
1510-089/PKS 1510-08	42.587 ± 0.036	44.019 ± 0.031	46.476 ± 0.300	45.750	-0.573 ± 0.129	8.347 ± 0.273	6.894 ± -0.923
1514-241	40.254 ± 0.036	42.020 ± 0.031	45.764 ± 0.300	44.500	-1.100 ± 0.129	7.649 ± 0.292	5.146 ± -1.439
B2 1520+31	43.048 ± 0.053	44.415 ± 0.045	47.034 ± 0.310	45.900	-0.566 ± 0.115	8.905 ± 0.283	7.464 ± -0.998
1546+027/PKS 1546+027	41.986 ± 0.036	43.504 ± 0.031	46.731 ± 0.300	45.670	-0.885 ± 0.129	8.614 ± 0.287	6.540 ± -1.227
4C+05.64	43.754 ± 0.036	45.020 ± 0.031	47.294 ± 0.300	46.057	-0.371 ± 0.129	9.144 ± 0.258	8.082 ± -0.734
4C+10.45	43.635 ± 0.036	44.918 ± 0.031	47.084 ± 0.300	46.006	-0.351 ± 0.129	8.931 ± 0.256	7.907 ± -0.716
1611+343/B2 1611+34	43.635 ± 0.019	44.917 ± 0.016	47.456 ± 0.300	46.870	-0.643 ± 0.144	9.332 ± 0.278	7.738 ± -0.999
1622-297	43.201 ± 0.036	44.545 ± 0.031	47.214 ± 0.300	48.780	-1.171 ± 0.129	9.099 ± 0.293	6.456 ± -1.509
1633+382/4C+38.41	43.833 ± 0.023	45.087 ± 0.020	47.483 ± 0.300	46.820	-0.555 ± 0.141	9.353 ± 0.273	7.933 ± -0.912
4C +47.44	43.102 ± 0.013	44.460 ± 0.011	46.679 ± 0.475	45.581	-0.373 ± 0.149	8.529 ± 0.438	7.463 ± -0.768
Mkn 501	39.879 ± 0.024	41.698 ± 0.021	46.951 ± 0.300	43.204	-1.321 ± 0.140	8.836 ± 0.295	5.894 ± -1.663
B3 1708+433	42.410 ± 0.068	43.867 ± 0.058	46.034 ± 0.350	45.032	-0.368 ± 0.102	7.883 ± 0.308	6.828 ± -0.504
1726+455	42.192 ± 0.036	43.681 ± 0.031	46.334 ± 0.300	45.850	-0.722 ± 0.129	8.212 ± 0.281	6.463 ± -1.068
1730-130	43.602 ± 0.036	44.890 ± 0.031	47.414 ± 0.300	45.830	-0.422 ± 0.129	9.271 ± 0.262	8.112 ± -0.781
1739+522	43.223 ± 0.039	44.564 ± 0.033	47.434 ± 0.300	46.160	-0.661 ± 0.127	9.310 ± 0.278	7.682 ± -1.007
4C+09.57/PKS1749+096	42.570 ± 0.036	44.005 ± 0.031	46.527 ± 0.300	44.699	-0.368 ± 0.129	8.377 ± 0.258	7.321 ± -0.731
CGRaBS J1800+7828	42.784 ± 0.008	44.188 ± 0.007	46.374 ± 0.300	45.851	-0.480 ± 0.153	8.237 ± 0.268	6.964 ± -0.848
3C 371	40.722 ± 0.007	42.421 ± 0.006	46.719 ± 0.300	43.000	-0.849 ± 0.155	8.601 ± 0.286	6.599 ± -1.204
1823+568/4C+56.27	43.017 ± 0.015	44.388 ± 0.013	47.374 ± 0.300	44.299	-0.332 ± 0.148	9.217 ± 0.255	8.231 ± -0.707
1849+670	42.492 ± 0.036	43.938 ± 0.031	47.254 ± 0.300	45.418	-0.763 ± 0.129	9.134 ± 0.283	7.303 ± -1.108
1921-293/PKS B1921-293	42.273 ± 0.036	43.751 ± 0.031	46.809 ± 0.300	45.020	-0.645 ± 0.129	8.684 ± 0.277	7.088 ± -0.992
2145+067/4C+06.69	43.409 ± 0.036	44.724 ± 0.031	46.984 ± 0.300	46.766	-0.583 ± 0.129	8.856 ± 0.274	7.381 ± -0.933
2155-152/PKS 2155-152	42.948 ± 0.036	44.329 ± 0.031	45.704 ± 0.300	44.682	0.032 ± 0.129	7.423 ± 0.203	7.095 ± -0.398
BL Lac	40.470 ± 0.036	42.204 ± 0.031	46.324 ± 0.300	43.519	-0.957 ± 0.129	8.207 ± 0.289	5.992 ± -1.297
PKS 2209+236	42.615 ± 0.036	44.044 ± 0.031	46.574 ± 0.450	45.786	-0.596 ± 0.129	8.446 ± 0.427	6.947 ± -1.458
2223-052/3C 446	44.516 ± 0.036	45.672 ± 0.031	46.531 ± 0.300	46.601	0.056 ± 0.129	8.237 ± 0.199	7.948 ± -0.381
PKS 2227-08	43.788 ± 0.036	45.049 ± 0.031	46.899 ± 0.300	46.664	-0.375 ± 0.129	8.749 ± 0.258	7.681 ± -0.737
2230+114/CTA 102	43.668 ± 0.036	44.946 ± 0.031	46.894 ± 0.300	46.870	-0.469 ± 0.129	8.756 ± 0.266	7.505 ± -0.825
2251+158/3C 454.3	43.860 ± 0.036	45.110 ± 0.031	46.939 ± 0.300	46.650	-0.352 ± 0.129	8.786 ± 0.256	7.761 ± -0.717
TXS 2331+073	41.628 ± 0.036	43.198 ± 0.031	46.484 ± 0.300	45.932	-1.025 ± 0.129	8.368 ± 0.490	6.017 ± -1.164
2345-16/PKS 2345-16	42.811 ± 0.036	44.211 ± 0.031	46.709 ± 0.300	45.359	-0.459 ± 0.129	8.570 ± 0.265	7.339 ± -0.815

Note: The first column is name; the second column is Logarithm of 151 MHz radio luminosity; the third column is Logarithm of beam power; the fourth column is the Logarithm of Eddington luminosity; the fifth column is Logarithm of the beaming factor; the sixth column is the Logarithm of the spin function; the seventh column is the Logarithm of black hole spin-mass energy; the eighth column is Logarithm of the black hole irreducible mass.

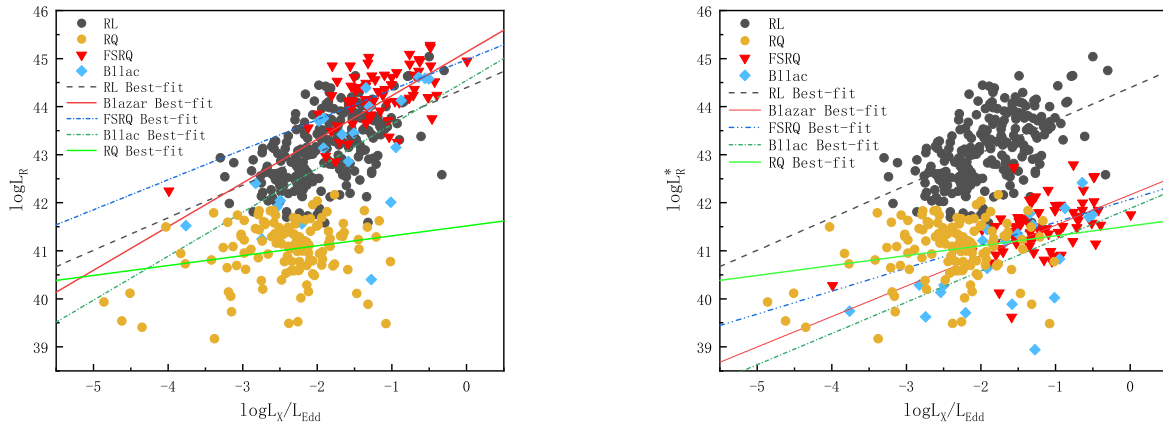


Figure 2. Left panel: The correlation between L_X/L_{Edd} and L_R . Right panel: The correlation between L_X/L_{Edd} and L_R with beaming corrected.

Table 3. The correlation analysis for L_R and $\frac{L_X}{L_{\text{Edd}}}$

Type	Best fit	R
RL	$\log L_R = 0.677 \pm 0.074 \log\left(\frac{L_X}{L_{\text{Edd}}}\right) + 44.396 \pm 0.147$	0.272
RQ	$\log L_R = 0.206 \pm 0.077 \log\left(\frac{L_X}{L_{\text{Edd}}}\right) + 41.518 \pm 0.193$	0.054
FSRQ	$\log L_R = 0.625 \pm 0.103 \log\left(\frac{L_X}{L_{\text{Edd}}}\right) + 44.977 \pm 0.139$	0.355
Bllac	$\log L_R = 0.909 \pm 0.115 \log\left(\frac{L_X}{L_{\text{Edd}}}\right) + 45.138 \pm 0.172$	0.391
Blazar	$\log L_R = 0.909 \pm 0.115 \log\left(\frac{L_X}{L_{\text{Edd}}}\right) + 45.138 \pm 0.172$	0.416
FSRQ*	$\log L_R = 0.478 \pm 0.107 \log\left(\frac{L_X}{L_{\text{Edd}}}\right) + 42.071 \pm 0.145$	0.229
BLLac*	$\log L_R = 0.651 \pm 0.205 \log\left(\frac{L_X}{L_{\text{Edd}}}\right) + 41.883 \pm 0.386$	0.347
Blazar*	$\log L_R = 0.634 \pm 0.095 \log\left(\frac{L_X}{L_{\text{Edd}}}\right) + 42.166 \pm 0.142$	0.338

Note: The R is R-Square as correlation coefficient; p is significance level; * indicates that the corresponding data has been corrected with beaming factor.

conducting the fundamental plane analysis of Blazars. The fundamental plane of Blazars after correcting anisotropism, $\log L_R = 0.190_{+0.049}^{-0.049} \log L_X + 0.475_{+0.157}^{-0.157} \log M + 28.568_{+2.245}^{-2.245}$ with R-Square=0.279, is showed in right plane of Figure 3. The existing FP relations from previous work (Saikia et al. 2018; Gultekin et al. 2019) are also included in Figure 3 for visualizing the results. The difference between our result and previous work has decreased after correcting anisotropism. This suggests that the fundamental plane of FSRQs are more similar to the fundamental plane of AGNs (Saikia et al. 2018) with beaming corrected. Both fundamental plane relations of Blazars are positive correlation and generally similar. However, there is a slight decrease in the R-Square of the fundamental plane, comparing to the original version, indicating that the beaming effect can have some impact on the fundamental plane analysis. The beaming effect enhances the role of jets in the fundamental plane relationship. The analysis results are showed in Table 4. The R-values (0.595 and 0.528) are above 0.5 and the significance of each variable is below the threshold of 0.05. The fitting results indicate that the correlation of fundamental plane for Blazars is strong. It supports the validity of the fundamental relationship. We also separately fitted FSRQs and BL Lacs by the same fundamental plane which is calculated by total sample. It can be observed that there are differences between the best-fitting lines of FSRQs and BL Lacs, and the best fit for the overall sample lies between these two. Furthermore, this characteristic remains even after the elimination of the beaming effect. The fundamental plane relationship still exists when Blazars and BL Lacs are discussed separately.

We also used redshift as third variable to conduct a partial correlation analysis of the correlation and discussed the effect of distance on result. The R-square value decreases from 0.279 to 0.232 and the significance level of both variables increased to 0.029 (still less than 0.05) after excluding the effect of redshift (distance) on the fundamental plane which has been corrected with beaming factor. It indicates that the result of fundamental plane is partly effected by distance. The correlation of fundamental plane still exists after removing the effect of distance from both the variables.

Table 4. The correlation analysis for the fundamental plane of Blazars

Type	R-Square	p(L_X)	p(M)	DW
Blazars	0.355	0.001	0.001	2.011
Blazars*	0.279	0.001	0.003	2.024

Note: R-Square is correlation coefficient; p(L_X) is significance level of $\log L_X$; p(M) is significance level of $\log M$; * indicates that the corresponding data has been corrected with beaming factor. DW is the Durbin-Watson statistic which is a statistical method used to assess the presence of autocorrelation in time series data.

Table 5. Correlation coefficient between L_X , L_R and M_{irr} , M_{spin}

Type	$\log L_X$ R-Square	$\log L_R$ R-Square	$\log L_{R^*}$ R-Square
M_{irr}	0.211	0.158	0.121
M_{spin}	0.362	0.604	0.501

3.2 fundamental plane of blazars base on BH spin energy

Before using BH spin energy as a variable for fundamental analysis, we need to discuss its effect on the black hole mass and its correlation with other variables. The relation between z and M_{dyn} , M_{irr} is presented in upper left panel of Figure 4. The differences between M_{dyn} and M_{irr} are evident. This is due to the contribution of M_{spin} (where $M \equiv M_{\text{dyn}} = M_{\text{irr}} + E_{\text{spin}} c^{-2} = M_{\text{irr}} + M_{\text{spin}}$), where the differences in mass are determined by the numerical value of the black hole spin. While the difference is negligible in samples with low spin, samples characterized by high spin exhibit a more significant discrepancy (Daly et al. 2022; Zhang et al. 2023a). The 3D correlation diagram: upper right panel, lower left panel and lower right panel in Figure 4, show that there are obvious correlations among $\log L_X$, $\log L_R$, $\log M_{\text{spin}}$ and $\log M_{\text{irr}}$. They are positively correlated with each other. The results of R-Square are listed in Table 5. This correlations existed after the effects of beam factors were taken into account. The analysis results indicate that the correlation observed in the fundamental plane relation of M_{dyn} is partly contributed by the M_{spin} . The analysis results also indicate that the correlation of black hole spin is more strongly correlated with the fundamental plane relation than irreducible black hole mass. It is important to analyze the role of black hole spin energy in the fundamental plane relation.

Consistent with Merloni et al. (2003), we examined the fundamental plane of Blazars based on M_{spin} . We replace the M_{dyn} variable with M_{irr} and M_{spin} , and discuss them separately in this paper. The results for new fundamental plane is showed in Table 6. After separately analyzing M_{spin} and M_{irr} , as shown in Figure 5. All the correlations are positive, and there are differences between the fundamental plane of M_{irr} and M_{spin} for Blazars. This may indicate that both M_{irr} and M_{spin} contribute to the correlation foundation for fundamental plane of Blazars. According to the results for new fundamental plane, M_{spin} contributes more correlation than M_{irr} . It means that the effect of BH spin on fundamental

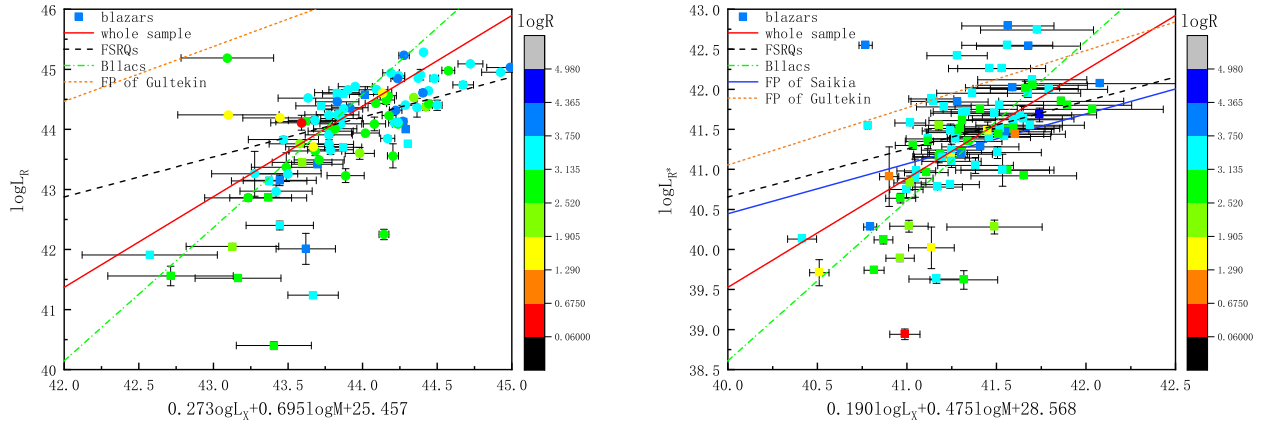


Figure 3. Left panel: The fundamental plane of Blazars. Right panel: The fundamental plane of Blazars with beaming corrected. R is the radio loudness. FP of Saikia is from Saikia et al. 2018, FP of Gultekin is from Gultekin et al. 2019.

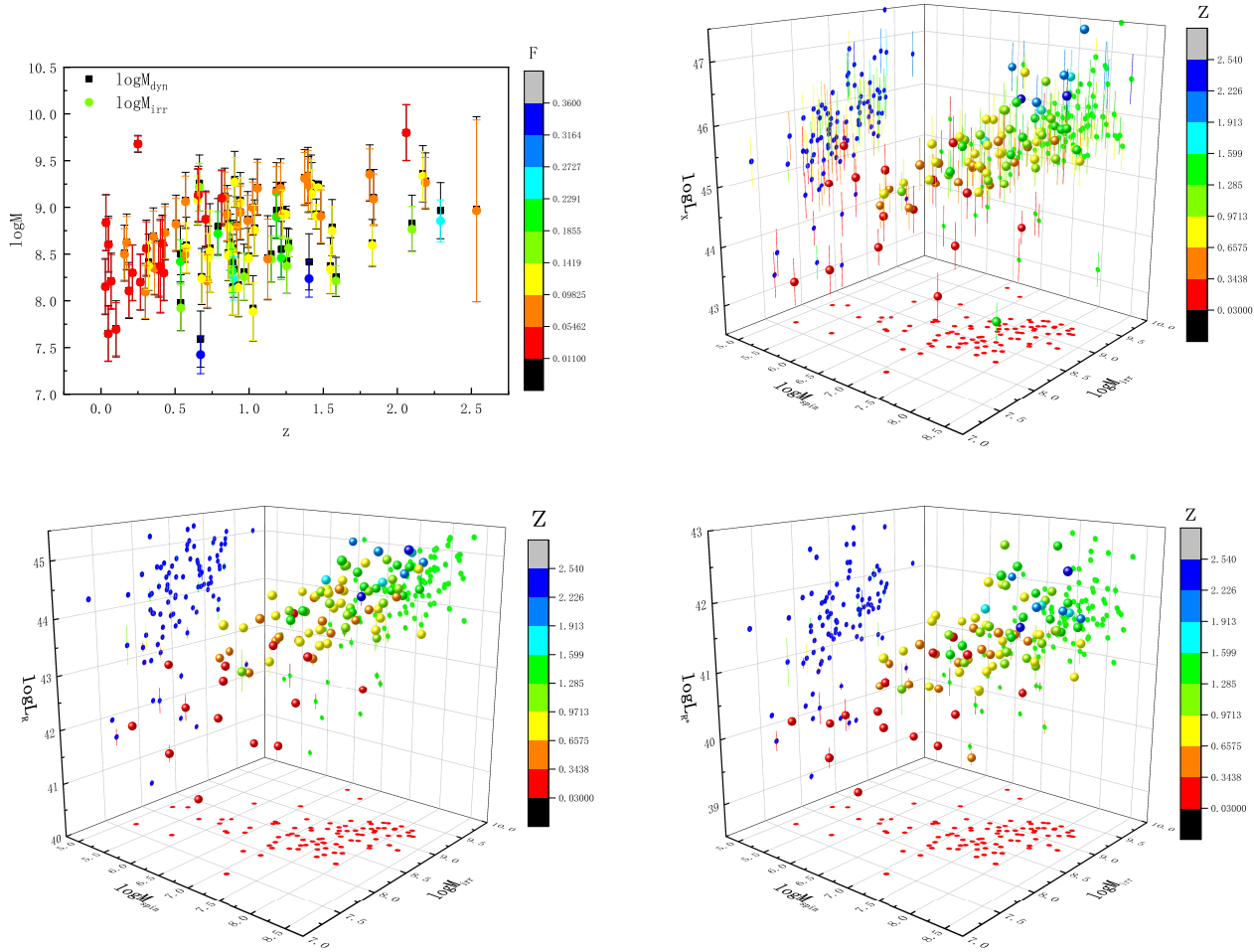


Figure 4. Upper left panel: The differences between $\log M_{\text{spin}}$ and $\log M_{\text{irr}}$. Upper right panel: The correlation between $\log L_X$, $\log M_{\text{spin}}$ and $\log M_{\text{irr}}$. Lower left panel: The correlation between $\log L_R$, $\log M_{\text{spin}}$ and $\log M_{\text{irr}}$. Lower right panel: The correlation between $\log L_{R^+}$, $\log M_{\text{spin}}$ and $\log M_{\text{irr}}$

Table 6. The correlation analysis for the fundamental plane based on M_{irr} and M_{spin}

Type(left plane)	R-Square	$p(L_X)$	$p(M_{\text{irr}})$	DW
Blazars*	0.429	0.001	0.010	1.9
Type(right plane)	R-Square	$p(L_X)$	$p(M_{\text{spin}})$	DW
Blazars*	0.575	0.001	0.001	1.7

Note: R-Square is correlation coefficient; $p(L_X)$ is significance of $\log L_X$; $p(M_{\text{irr}})$ is significance of $\log M_{\text{irr}}$; $p(M_{\text{spin}})$ is significance level of $\log M_{\text{spin}}$; * indicates that the corresponding data has been corrected with beaming factor. DW is the Durbin-Watson statistic which is a statistical method used to assess the presence of autocorrelation in time series data.

plane is relatively large. Since XRBs apply to fundamental relationships and its jet mechanism is also similar to AGNs. This effect is similar to the radio loud and radio quiet sources in the $L_r - L_x$ correlation of XRBs (Fender et al. 2003; Gallo et al. 2003) for the sources of XRBs which have black hole spins. Therefore, it is necessary to discuss the effect of M_{spin} on the traditional fundamental plane and consider the M_{spin} as a important factor for the study of fundamental plane.

4 CONCLUSIONS

In this paper, we repeated the fundamental plane of previous work (Merloni et al. 2003) with Blazars. A total of 91 samples were obtained through sample collection. We examined a traditional fundamental plane of black hole activity for Blazars. The fundamental plane is $\log L_R = 0.273_{+0.059}^{-0.059} \log L_X + 0.695_{+0.191}^{-0.191} \log M + 25.457_{+2.728}^{-2.728}$ with R-Square=0.355. Although this fundamental plane is similar to the previous work of AGN in general (Merloni et al. 2003; Unal et al. 2015; Bariuan et al. 2022), there are quite differences in the coefficients. The fundamental plane for our Blazars after considering the effect of beam factor is $\log L_R = 0.190_{+0.049}^{-0.049} \log L_X + 0.475_{+0.157}^{-0.157} \log M + 28.568_{+2.245}^{-2.245}$ with R-Square=0.279. The fundamental plane of Blazars with beaming effect corrected is more similar to the radio-quiet quasars of previous work (Bariuan et al. 2022). This could be attributed to the jet opening angles of Blazars, which results in a significant influence of beaming effect on the jet emission. The work of Bariuan et al. (2022) has indicated that radio loudness has an impact on the fundamental plane within quasar samples. To accurately model the dichotomy between radio-loud and radio-quiet quasars, two different fundamental plane models are required. It has been previously concluded that radio-loud and radio-quiet quasars may be governed by distinct fundamental plane models (Bariuan et al. 2022). Typically, the emission mechanism for radio-quiet samples is dominated by accretion flows, while radio-loud samples are likely a combination of jet and disk. However, in this study, as shown in Figure 2, our Blazars tend to exhibit characteristics of radio-loud samples before correcting anisotropism, while their characteristics lean towards radio-quiet samples after considering the effect of beam factor. We speculate that the difference in jet opening angles leads to the manifestation of both jet-

dominated and accretion disk-dominated fundamental plane models for Blazars. Due to the fact that all samples are radio-loud objects, and the distribution of radio loudness data points in Figure 3 wasn't affected by the beaming effect. We found that Blazars are more suitable for the jet-dominated fundamental plane models.

Standard fundamental models can accurately describe the production of black hole jets (Unal et al. 2015), but they still have some deviations. In this paper, we consider the influence of black hole spin to reduce these deviations in the fundamental models. As the spin increases, a larger portion of the gravitational energy can be converted into radiation due to the closer proximity of accreted matter to the event horizon. The correlation indicates a positive relationship between the jet power and the black hole spin-mass energy, which is validated by correlation analysis. Therefore, the effect of black hole spin should be considered for the study of fundamental plane. To improve accuracy of conclusion, our goal is to include as many variables as possible. Thus, we introduce M_{spin} as a variable in the fundamental model, which is calculated by the spin and mass of BH. The new fundamental plane in this paper ($\log L_R = 0.332_{+0.081}^{-0.081} \log L_X + 0.502_{+0.091}^{-0.091} \log M_{\text{spin}} + 22.606_{+3.346}^{-3.346}$ with R-Square=0.575) shows that the fundamental plane based on M_{spin} has a stronger relation compared to the fundamental plane based on the mass of BH also known as M_{dyn} ($\log L_R = 0.190_{+0.049}^{-0.049} \log L_X + 0.475_{+0.157}^{-0.157} \log M + 28.568_{+2.245}^{-2.245}$ with R-Square=0.279). Hence, the parameter M_{spin} holds significant importance in the fundamental plane of Blazars (Zhang et al. 2023a). Our findings underscore the crucial role of black hole spin in the accretion and outflow processes (Unal et al. 2015). We confirmed the correlation among jet, accretion, and spin of BH which indicates the applicability of BZ model for Blazars. It is consistent with the conclusions of previous work (Blandford et al. 1977, 2019; Unal et al. 2015) and could provide a observational indication for the existence of the Blandford-Znajek process.

Due to the flux variation of Blazars, the observed value of the sample will change with time, especially for radio luminosity, if the observation time interval is large, it may produce errors, which will affect the fundamental plane analysis results. This change may cause the correlation of R-Square to decrease. Agns and blazars have different bands of radiation that are correlated with each other and there is a significant time lag between these radiations (Xie et al. 2017). In order to improve the accuracy of the analysis results, we limited the observation time of the collected data sources in 2-5 years. However, the time interval between radio and X-ray emissions in Blazars generally ranges from months to years. AGNs exhibit variability, with the potential for amplitude reaching approximately 100% on timescales that are shorter than the observation time interval (Ho et al. 2001). This uncertainty may govern the actual observed uncertainty of flux (Xie et al. 2017). Therefore, to investigate the intrinsic and physically related Fundamental Plane, it is important to account for the radio/X-ray time interval. But implementing such a correction for Blazars is exceedingly difficult due to the requirement of long-term, coordinated monitoring of individual sources in both radio and X-ray bands (Xie et al. 2017). Additionally, this monitoring must capture at least one outburst in each Blazars to obtain a dependable timelag measurement. Consequently, only a limited number of AGNs

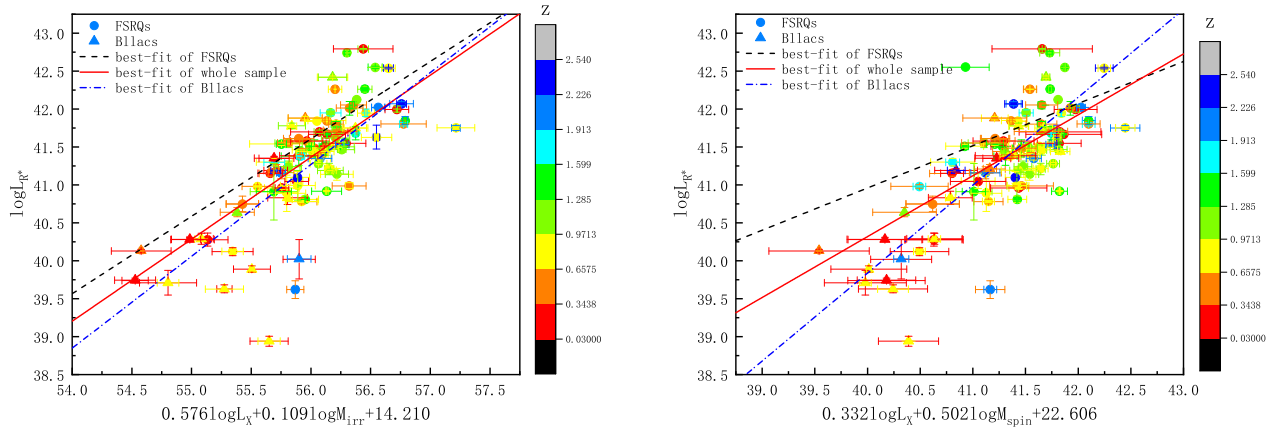


Figure 5. Left panel: The fundamental plane of Blazars based on $\log M_{\text{irr}}$ after beam-correction. Right panel: The fundamental plane of Blazars based on $\log M_{\text{spin}}$ after beam-correction.

have undergone such intensive monitoring to date, as it poses significant challenges (Bell et al. 2011; King et al. 2013). In this paper the uncertainty because of non-simultaneous (radio and X-ray) observations we taken is from Ho et al. (2001) which adopted a slightly smaller scatter in radio luminosities (0.2 dex).

ACKNOWLEDGMENTS

We gratefully thank the anonymous referee for the very helpful comments, which helped us to greatly improve this paper. This work is partially supported by Natural Science Foundation of Yunnan(202101AU070006), National Natural Science Foundation of China (12063006), Young and middle-aged academic and technical reserve talents of Yunnan Province (202205AC160087) and Yunnan Provincial Department of Education Research Fund (2021J0671). The authors gratefully acknowledge the computing support provided by the JRT Science Data Center at Yuxi Normal University. QLH gratefully acknowledges the financial support from the Hundred Talents Program of Yuxi (grant 2019).

DATA AVAILABILITY

The data underlying this article are available in the article and in its online supplementary material.

REFERENCES

Abdo, A. A., Ackermann, M., Ajello, M., et al. 2010, ApJS, 188, 405. <https://doi.org/10.1088/0067-0049/188/2/405> 2

Ackermann, M., Ajello, M., Albert, A., et al. 2011, ApJ, 743, 171. <https://doi.org/10.1088/0004-637X/743/2/171> 2

Bariuan, L. G., Snios, B., Sobolewska, M., et al. 2022, MNRAS, 513, 4673. <https://doi.org/10.1093/mnras/stac1153> 2, 7, 12

Begelman, M. C., Blandford, R. D., Rees, M. J., 1984, Rev. Mod. Phys, 56, 255. <https://doi.org/10.1103/RevModPhys.56.255> 1, 2

Bell, M. E., Tzioumis, T., Uttley, P., et al. 2011, MNRAS, 411, 402. <https://doi.org/10.1111/j.1365-2966.2010.17692.x> 13

Blandford, R. D., Znajek, R. L., 1977, MNRAS, 179, 433. <https://doi.org/10.1093/mnras/179.3.433> 2, 7, 12

Blandford, R. D., Rees, M. J., 1978, in Wolfe A. M., ed., Pittsburgh ConferBence on BLLac Objects. Univ. Pittsburgh press, Pittsburgh, p. 328. <https://babel.hathitrust.org/cgi/pt?id=uc1.b4520824&view=1up&seq=328> 2

Blandford, R. D. 1990, in Active Galactic Nuclei, ed. T. J. L. Courvoisier & M. Mayor (Berlin:Springer), 161. <https://ui.adsabs.harvard.edu/abs/1990agn...conf..161B/abstract> 4

Blandford, R., Meier, D., Readhead, A., 2019, ARA& A, 57, 467. <https://doi.org/10.1146/annurev-astro-081817-051948> 12

Cao, X., Jiang, D. R. 1999, MNRAS, 307, 802. <https://doi.org/10.1046/j.1365-8711.1999.02657.x> 2

Cao, X. W. 2003, ApJ, 599, 147. <https://doi.org/10.1086/379240> 4

Calderone, G., Ghisellini, G., Colpi, M. & Dotti, M. 2013, MNRAS, 431, 210. <https://doi.org/10.1093/mnras/stt157> 4

Celotti, A., Padovani, P., Ghisellini, G., 1997, MNRAS, 286, 415. <https://doi.org/10.1093/mnras/286.2.415> 4

Chai, B., Cao, X. W., Gu, M. F., 2012, ApJ, 759, 114. <https://doi.org/10.1088/0004-637X/759/2/114> 2, 3

Daly, R. A., Stout, D. A., Mysliwiec, J. N. 2018, ApJ, 863, 117. <https://doi.org/10.3847/1538-4357/aad08b> 4

Daly, R. A. 2019, ApJ, 886, 37. <https://doi.org/10.3847/1538-4357/ab35e6> 4

Daly, R. A. 2022, MNRAS, 517, 5144. <https://doi.org/10.1093/mnras/stac2976> 2, 4, 10

Falcke, H., Biermann, P. L., 1994, A&A, 293, 665. <https://doi.org/10.48550/arXiv.astro-ph/9411096> 1

Falcke, H., Körding, E., Markoff, S. 2004, A&A., 414, 895.

- <https://doi.org/10.1051/0004-6361:20031683> 1, 2
- Fan, X. L., Wu, Q. 2018, ApJ, 869, 133. <https://doi.org/10.3847/1538-4357/aaeece> 4
- Fender, R. P., Gallo, E., Jonker, P. G. 2003, MNRAS, 343, L99. <https://doi.org/10.1046/j.1365-8711.2003.06950.x> 12
- Fan, X. L., Wu, Q. 2019, ApJ, 879, 107. <https://doi.org/10.3847/1538-4357/ab25f1> 4
- Fichtel, C. E., Bertsch, D. L., Chiang, J., et al. 1994, ApJS, 94, 551. <https://doi.org/10.1086/192082> 2
- Francis, P. J., Hewett, P. C., Foltz, C. B., et al. 1991, ApJ, 373, 465. <https://doi.org/10.1086/170066> 4
- Gallo, E., Fender, R. P., Pooley, G. G. 2003, MNRAS, 343, 60. <https://doi.org/10.1046/j.1365-8711.2003.06791.x> 12
- Garofalo, D., Meier, D. L. 2010, MNRAS, 406, 2047. <https://doi.org/10.1111/j.1365-2966.2010.16815.x> 2
- Ghisellini, G., Tavecchio, F., Foschini, L., et al. 2010, MNRAS, 402, 497. <https://doi.org/10.1111/j.1365-2966.2009.15898.x> 2
- Ghisellini, G., Tavecchio, F., Maraschi, L., Celotti, A., Sbarrato, T. 2014, Nature, 515, 376. <https://doi.org/10.1038/nature13856> 2
- Godfrey, L. E. H., Shabala, S. S. 2013, ApJ, 767, 12. <https://doi.org/10.1088/0004-637X/767/1/12> 4
- Gultekin, K., Cackett, E. M., Miller, J. M., et al. 2009, ApJ, 706, 404. <https://doi.org/10.1088/0004-637X/706/1/404> 1, 2
- Gultekin, K., King, A. L., Cackett, E. M., et al. APJ, 871, 80. <https://iopscience.iop.org/article/10.3847/1538-4357/aaf6b9> 10
- Gu, M. F., Cao, X. W., Jiang, D. R., 2009, MNRAS, 396, 984. <https://doi.org/10.1111/j.1365-2966.2009.14758.x> 2
- Heinz, S., Sunyaev, R. A. 2003, MNRAS, 343, L59. <https://doi.org/10.1046/j.1365-8711.2003.06918.x> 2
- Ho, L. C., Peng, C. Y. 2001, APJ, 555, 650. <https://iopscience.iop.org/article/10.1086/321524> 12, 13
- King, A. L., Miller, J. M., Reynolds, M. T., et al. 2013, ApJL, 774, L25 <https://dx.doi.org/10.1038/nphys3724> 13
- Körding, E., Falcke, H., Corbel, S. 2006, A&A, 456, 439. <https://doi.org/10.1051/0004-6361:20054144> 1, 2, 7
- Körding, E., Fender, R., Migliari, S. 2006, MNRAS, 369, 1451. <https://doi.org/10.1111/j.1365-2966.2006.10383.x> 1
- Liu, Y., Jiang, D. R., Gu, M. F., 2006, ApJ, 637, 669. <https://doi.org/10.1086/498639> 2, 3
- Leon, T. J., Valtaoja, E., Chavushyan, V. H., et al. 2011, MNRAS, 411, 1127. <https://doi.org/10.1111/j.1365-2966.2010.17740.x> 2, 3
- Meier, D. L., 2001, ApJ, 548, L9. <https://doi.org/10.1086/318921> 2
- Meier, D. L., 2002, New Astron. Rev, 46, 247. [https://doi.org/10.1016/S1387-6473\(01\)00189-0](https://doi.org/10.1016/S1387-6473(01)00189-0) 2
- Merloni, A., Heinz, S., Matteo, T. 2003, MNRAS, 345, 1057. <https://doi.org/10.1046/j.1365-2966.2003.07017.x> 1, 2, 4, 7, 10, 12
- Miller, J. M., Reynolds, C. S., Fabian, A. C., Miniutti, G., Gallo, L. C. 2009, ApJ, 697, 900. <https://doi.org/10.1088/0004-637X/697/1/900> 4
- Misner, C. W., Thorne, K. S., Wheeler, J. A. 1973, Gravitation (San Francisco: W.H.Freeman and Company), 3. <https://ui.adsabs.harvard.edu/abs/1973grav.book.....M/abstract> 4
- Nemmen, R. S., Georganopoulos, M., Guiriec, S., et al. 2012, Science, 338, 1445. <https://doi.org/10.1126/science.1227416> 2, 3
- Netzer, H. 1990, in Active Galactic Nuclei (Berlin: Springer) ,57. <https://ui.adsabs.harvard.edu/abs/1990agn.conf...57N/abstract> 4
- Nolan, P.L., Abdo, A. A., Ackermann, M., Ajello, M., et al. 2012, ApJS, 199, 31. <https://doi.org/10.1088/0067-0049/199/2/31> 2
- Plotkin, R. M., Markoff, S., Kelly, B. C., Koerding, E., Anderson, S., F. 2012, MNRAS, 419, 267. <https://doi.org/10.1111/j.1365-2966.2011.19689.x> 2
- Rawlings, S., Saunders, R., 1991, Nature, 349, 138. <https://doi.org/10.1038/349138a0> 2
- Reynolds, C. S. 2014, SSRv, 183, 277. <https://doi.org/10.1007/s11214-013-0006-6> 4
- Rees, M. J. 1984, ARA&A, 22, 471. <https://doi.org/10.1146/annurev.aa.22.090184.002351> 4
- Saikia, P., K rding, E., Falcke, H. 2015, MNRAS, 450, 2317. <https://doi.org/10.1093/mnras/stv731> 2
- Saikia, P., K rding, E., Falcke, H. 2016, MNRAS, 461, 297. <https://doi.org/10.1093/mnras/stw1321> 2
- Saikia, P., Kording, E., Coppejans, Deanne L., et al. 2018, A&A, 616, 15 <https://doi.org/10.1051/0004-6361/201833233> 10
- Sahakyan, N., Giommi, P. 2021, MNRAS, 502, 836 <https://doi.org/10.1093/mnras/stab011> 3
- Sbarrato, T., Ghisellini, G., Maraschi, L., Colpi, M., 2012, MNRAS, 421, 1764. <https://doi.org/10.1111/j.1365-2966.2012.20442.x> 2, 3, 4
- Scarpa, R., Falomo, R., 1997, A&A, 325, 109. <https://articles.adsabs.harvard.edu/pdf/1997A%26A...325..109S> 2
- Shaw, M. S., Romani, R. W., Cotter, G., et al. 2012, ApJ, 748, 49. <https://doi.org/10.1088/0004-637X/748/1/49> 2, 3
- Shen, Y., Liu, X., Greene, J. E., et al. 2011, ApJS, 194, 45. <https://doi.org/10.1088/0067-0049/194/2/45> 2, 3
- Tavecchio, F., Ghisellini, G., Ghirlanda, G., Foschini, L., Maraschi, L., 2010, MNRAS, 401, 1570. <https://doi.org/10.1111/j.1365-2966.2009.15784.x> 2
- Thorne, K. S., Price, R. H., Macdonald, D. A., Suen, W. M., Zhang, X. H., 1986, in Black Holes: The Membrane Paradigm(New Haven: Yale University Press), 67. <https://ui.adsabs.harvard.edu/abs/1986bhmp.book...67T/abstract> 4
-  nal, C., Loeb, A. 2015, MNRAS, 495, 278. <https://doi.org/10.1093/mnras/staa1119> 1, 2, 7, 12
- Urry, C. M., Padovani, P., 1995, PASP, 107, 803. <https://doi.org/10.1086/133630> 2
- Vestergaard, M., Osmer, P. S., 2009, ApJ, 699, 800. <https://doi.org/10.1088/0004-637X/699/1/800> 3
- Vestergaard, M., Peterson, B. M., 2006, ApJ, 641, 689. <https://doi.org/10.1086/500572> 3
- Wang, J. Min; Luo, B; Ho, L. C., 2014, ApJ, 797, 65. <https://doi.org/10.1088/0004-637X/797/1/65> 2, 3
- Wang, F. Y., & Dai, Z. G., 2017, MNRAS, 470, 1101. <https://doi.org/10.1093/mnras/stx1292> 7
- Wu, Q., Cao, X. 2008, ApJ, 678, 156. <https://doi.org/>

- [10.1086/591933](https://doi.org/10.1086/591933) 4
- Woo, J. H., Urry, C. M., 2002, ApJ, 579, 530. <https://doi.org/10.1086/342878> 2, 3
- Willott, C. J., Rawlings, S., Blundell, K. M., et al. 1999, MNRAS, 309, 1017. <https://doi.org/10.1046/j.1365-8711.1999.02907.x> 4
- Xie, G. Z., Liu, F. K., Liu, B. F., et al. 1991, A&A, 249, 65. <https://articles.adsabs.harvard.edu/pdf/1991A%26A...249...65X> 3
- Xie, G. Z., Zhou, S. B., Liang, E. W., 2004, AJ, 127, 53. <https://doi.org/10.1086/380218> 2, 3
- Xie, F. Z., Yuan, F., 2017, AJ, 836,104. <https://doi.org/10.3847/1538-4357/aa5b90> 12
- Xiong, D. R., Zhang, X. 2014, MNRAS, 441, 3375. <https://doi.org/10.1093/mnras/stu755> 3, 4
- Xiong, D. R., Zhang, X., Bai, J. M., Zhang, H. J., 2015, MNRAS, 450, 3568. <https://doi.org/10.1093/mnras/stv812> 2
- Zhang, X., Zhang, H. J., Zhang, X., Xiong, D. R. 2017, Ap&SS, 362, 244. <https://doi.org/10.1007/s10509-017-3199-4> 3
- Zhang, X., Zhang, H. J., Zhang, X. 2018, Ap&SS, 363, 259. <https://doi.org/10.1007/s10509-018-3478-8> 2, 7
- Zhang, J., Liang, E. W., Zhang, S. N., Bai, J. M., 2012, ApJ, 752, 157. <https://doi.org/10.1088/0004-637X/752/2/157> 2, 3
- Zhang, X., Gao, Q. G., 2023, Ap&SS, 368, 69. <https://doi.org/10.1007/s10509-023-04225-y> 3, 4, 7, 10, 12
- Zhang, X., Gao, Q. G., 2023, RAA, 23, 125019. <https://doi.org/10.1088/1674-4527/ad020c> 3
- Zhou, M., Cao, X., 2009, RAA, 9, 293. <https://doi.org/10.1088/1674-4527/9/3/003> 2, 3